Journal of the Mechanical Behavior of Biomedical Materials 78 (2018) 46–55

Contents lists available at ScienceDirect

Journal of the Mechanical Behavior of Biomedical Materials

journal homepage: www.elsevier.com/locate/jmbbm

Comparison of microsphere penetration with LC Bead LUMI™ *versus* other commercial microspheres

Marcus Caine[a,b], Xunli Zhang[b], Martyn Hill[b], Wei Guo[a], Koorosh Ashrafi[a], Zainab Bascal[a], Hugh Kilpatrick[a], Anthony Dunn[a], David Grey[a], Rosemary Bushby[a], Andrew Bushby[c], Sean L. Willis[a], Matthew R. Dreher[a], Andrew L. Lewis[a,*]

[a] *Biocompatibles UK Ltd, a BTG Group Company, Lakeview, Riverside Way, Watchmoor Park, Camberley GU15 3YL, UK*
[b] *Faculty of Engineering and the Environment, University of Southampton, University Road, Highfield, Southampton SO17 1BJ, UK*
[c] *School of Engineering and Materials Science, Queen Mary University, Mile End Road, London E1 4NS, UK*

ARTICLE INFO

Keywords:
Embolization microspheres
Penetration plate model
Renal embolization model
Compressive modulus

ABSTRACT

The purpose of this study was to evaluate LC Bead LUMI™ (40–90 μm and 70–150 μm) in order to determine if their increased resistance to compression influences microsphere penetration and distribution compared to more compressible commercial microspheres. LC Bead LUMI™ 40–90 μm and 70–150 μm, LC Bead*M1*® 70–150 μm, Embozene™ 40 μm and Embozene™ 100 μm size and distributions were measured using optical microscopy. Penetration *in vitro* was evaluated using an established 'plate model', consisting of a calibrated tapered gap between a glass plate and plastic housing to allow visual observation of microsphere penetration depth. Behaviour *in vivo* was assessed using a rabbit renal embolization model with histopathologic confirmation of vessel penetration depth. Penetration behaviour *in vitro* was reproducible and commensurate with the measured microsphere size, the smaller the microsphere the deeper the penetration. Comparison of the microsphere diameter measured on the 2D plate model *versus* the corresponding average microsphere size measured by histopathology in the kidney showed no significant differences ($p = > 0.05$ Mann-Whitney, demonstrating good *in vitro* - *in vivo* predictive capabilities of the plate model) confirming predictable performance for LC Bead LUMI™ (40–90 μm and 70–150 μm) based on microsphere size, their increased rigidity having no bearing on their depth of penetration and distribution. An assessment of a LC Bead LUMI™ (40–90 μm and 70–150 μm) has shown that despite having greater resistance to compression, these microspheres behave in a predictable manner within *in vitro* and *in vivo* models comparable with more compressible microspheres of similar sizes.

1. Introduction

Evaluation of physicomechanical properties has been recognized as an important performance predictor for embolic microspheres. One major attribute typically reported is the compressibility or compressive modulus of microspheres (a measure of their resistance to being compressed when delivered through a microcatheter for instance), with several methods described in the literature that compress either a monolayer of microspheres (Forster et al., 2010; Hidaka et al., 2011; Jordan et al., 2010; Lewis et al., 2006, 2007) or single microspheres themselves (Duran et al., 2016; Hidaka et al., 2010). This measure in-itself does not allow any prediction of the behaviour of microspheres in confined microvascular structures and can be difficult to interpret in isolation. Another issue that arises is in the testing of smaller (< 100 μm) or highly compressible microspheres, where it can be increasingly difficult to define the compressive modulus in an accurate and reproducible manner utilizing mechanical force compression methods. The implementation of novel characterization methods designed to predict dynamic *in vivo* flow behaviour is one proposed solution to this issue. Examples of such methods have been recently reported in the literature and present in the form of flow-modelling devices and tests for penetration efficacy and occlusion potential (Duran et al., 2016; Caine et al., 2016; Lewis et al., 2016).

LC Bead LUMI™ is a microspherical radiopaque embolization agent that has been designed to be visualized under conventional X-ray imaging techniques to provide the physician with real-time intra-procedural and post-procedural information on microsphere location (Duran et al., 2016; Levy et al., 2016; Sharma et al., 2016). The preparation of these microspheres has been previously described in detail and shows that the introduction of the radiopaque moieties into the

* Corresponding author.
E-mail address: andrew.lewis@btgplc.com (A.L. Lewis).

https://doi.org/10.1016/j.jmbbm.2017.10.034
Received 31 August 2017; Received in revised form 27 October 2017; Accepted 30 October 2017
Available online 31 October 2017

microsphere structure increases the material density and stiffness by several orders of magnitude compared to existing microspherical agents (Duran et al., 2016). Delivery of these products through a microcatheter is uncomplicated as they are used in pure contrast agent to ensure good suspension despite their dense nature and with a recommended dilution of at least 1 mL of microsphere sediment in 10 mL of contrast agent. Despite this, the maximum size range available is 100–300 μm, with the overwhelming number of clinical cases so far being conducted with the 70–150 μm size range due to preferred imaging outcome from the more distal penetration in the vessels. This finding has led to the release of a new size range (LC Bead LUMI™ 40–90 μm) that provides the potential for even more distal penetration into tumors. Given the known increase in compressive modulus for these products, however, the question arises as to whether the increased stiffness of the microspheres will limit their distal penetration potential.

In this study we present comparative *in vitro* evaluation using a flow-modelling method together with the *in vivo* correlation for two LC Bead LUMI™ size ranges (40–90 μm and 70–150 μm) *versus* LC Bead*M1*® (70–150 μm) and two sizes of Embozene™ microspheres (40 μm and 100 μm) which are of similar size but more compressible in nature. This study seeks to better understand the influence of a microspheres compressive modulus on its penetration behaviour.

2. Materials and methods

2.1. Test products

LC Bead LUMI™ 40–90 μm (LUMI 40–90) and LC Bead LUMI™ 70–150 μm (LUMI 70–150) (Biocompatibles UK Ltd, Farnham, UK) were compared to LC Bead*M1*® (LC 70–150) (Biocompatibles UK Ltd, Farnham, UK) and Embozene™ microspheres 40 μm (EZ 40) and 100 μm (EZ 100) (Boston Scientific, USA) as bench marks. The microspheres were prepared and used in the various evaluations as per the manufacturers' instructions for use (IFU). For LC Bead LUMI, iodinated contrast agent (Omnipaque 350™, GE Healthcare, UK) was utilised undiluted for suspension, whereas LC Bead*M1*® and Embozene™, a dilution of 50:50 contrast to saline was employed.

2.2 Optical sizing

Microspheres plus packing solution were transferred from their original packaging into a petri dish as a monolayer and sizing was accomplished using an Olympus BX50 microscope equipped with a ColorView III camera (Olympus, Japan). Sizing was performed manually on a population of at least n = 200 microspheres randomly over several fields of view using the sizing tool provided in the AnalySIS software package (Soft Imaging Systems GmbH, Germany). Size information was reported as a frequency distribution and also reported as average, minimum and maximum microsphere size, together with accompanying images for morphological assessment.

2.3. Evaluation of individual microsphere compressive modulus

Mechanical testing of microspheres was achieved by compressing individual microspheres up to 30% of their diameter using a UMIS 2000 nanoindentation system (CSIRO Instruments, Lindfield NSW, Australia) operated by IBIS software (Fischer-Cripps Laboratories Pty, NSW, Australia) with a force range of 0.01–45 mN and displacement range 1 nm to 150 μm, as previously described in detail (Duran et al., 2016). A sample of microspheres was dispersed in a dish and submerged in saline. Individual microspheres were selected using the optical microscope on the UMIS instrument and their diameters measured to the nearest 5 μm. Individual microspheres were then compressed at rates in the range (~ 3%diameter/s). Loading was completed in 10 s, where achievable. The compression modulus of each bead was calculated from the loading curve, applying linear elastic Hertzian contact mechanics for the case of a sphere compressed between two flat surfaces. The test was repeated on 15 individual beads giving a statistical sample with a t-distribution within 10% of the normal distribution at the 95% confidence level.

2.4. 2D penetration efficiency model for prediction of distal penetration

A 2D plate model, as described previously (Duran et al., 2016; Lewis et al., 2016) was used for distribution profiling of embolic microsphere penetration in a range between 25 and 555 μm. The model comprised of a milled Delrin™ channel with cover glass plate providing a gap with a diminishing internal diameter. A hydrostatic pressure of 40 mmHg was established to emulate circulatory blood pressure in appropriately sized vessels (hepatic pressure varying from 90 mmHg in the hepatic artery to 10 mmHg in the sinusoids with microspheres generally residing in vessels mid-size to these extremes (Khurana, 2006)). A slurry of 0.1 mL settled microspheres was introduced *via* an injection port using a 3 mL syringe (BD, USA) into the carrier fluid line, whereby the fluid flow (under hydrostatic pressure) carried the microspheres into the plate assembly until they were physically constrained by their size and could not migrate further into the narrowing gap. From this position it was possible to extract the positional length travelled at the furthest point "distal" to the injection site and "proximal". A picture of the plate assembly was captured using a digital camera and the microsphere blocking point and distribution of microspheres throughout the plate assembly noted in centimetres and converted accordingly to internal micrometer diameter (Fig. 1).

2.5. Microsphere suspension preparation

Microsphere suspensions for *in vivo* use were prepared by mixing the beads with a mixture 20/80 of saline/contrast (Omnipaque 350™, GE Healthcare, UK) to reach a final dilution of 1:20. The volume of saline and contrast added to the vial/syringe of bead is presented in Table 1.

2.6. Microsphere distribution in vivo using a kidney embolization model

The *in vivo* experiments were performed by Archimmed SARL at the Centre de Recherche en Imagerie Interventionelle (CR2i; Jouy en Josas

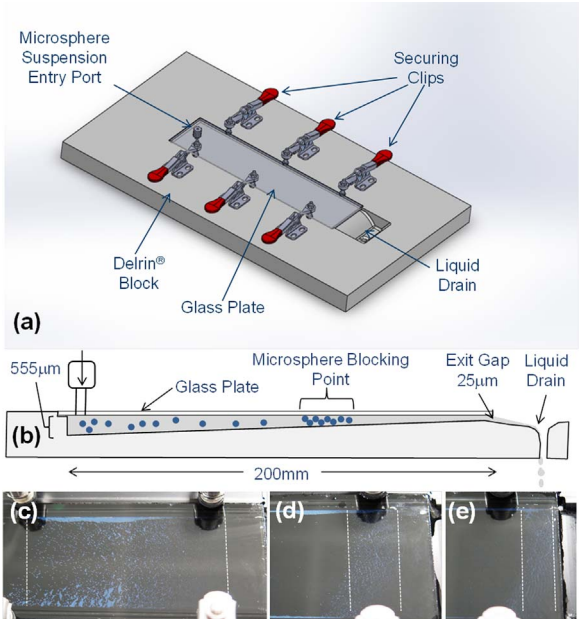

Fig. 1. (a) Representative schematic of the 2D plate penetration efficacy model; (b) side profile of the model; photographs of (c) 100–300 μm (d), 70–150 μm and (e) 40–90 μm size range band distributions of LC Bead LUMI™ on the model.

Table 1
Dilution of microsphere types prior to renal administration.

Product	Size (μm)	Bead volume (mL)	Saline volume (mL)	Total volume (mL)	Saline volume (mL)	Contrast volume (mL)
LUMI 40–90	40–90	2.0	6.0	34.0	6.8	27.2
LUMI 70–150	75–150	2.0	6.0	34.0	6.8	27.2
LC 70–150	75–150	2.0	6.0	34.0	6.8	27.2
EZ 40	40	2.0	5.0	35.0	7.0	28.0
EZ 100	100	2.0	5.0	35.0	7.0	28.0

Cedex, France). The CR2i complies with the French regulation regarding experiments on live animals: Decree No. 2013-118 dated 2013 February 1st from the French Ministry of Food and Forestry, on the protection of animals used for scientific purposes. The protocol was reviewed by the local ethics committee (COMETHEA Comité d'Ethique appliqué à l'Expérimentation Animale du Centre INRA de Jouy-en-Josas et d'AgroParisTech) under the number #14–54 and received positive notification without modification or reservation (notification dated 20th January 2015).

The kidney embolization model has been used previously to assess the arterial distribution of calibrated embolic microspheres and particles in the sheep (Laurent et al., 2006; Verret et al., 2011), swine (Stampfl et al., 2009; Maeda et al., 2013a) and in the rabbit (Weng et al., 2013). Whilst the sheep and swine models offer vessels sizes more akin to that in found in humans, the microspheres evaluated in this study were of the smallest size ranges used in embolization procedures with some overlap in their size ranges (40–90 μm and 70–150 μm) and arterial distribution was therefore evaluated in the rabbit renal artery embolization model where vessel sizes are smaller and more likely to enable differences between products to be discerned.

A total of 9 male White New Zealand rabbits were used for the study. All of the animals were > 5 months of age (50 ± 19 weeks, min max 31–98 weeks) and weighted more than 3.0 kg (3.920 ± 0.250 kg, min-max 3.350–4.250 kg). Vascular access to the right femoral artery was performed surgically after incision of the hind muscle and exposure of the femoral artery. A 4 French vascular sheath was inserted in the artery and a 4 Fr catheter was used to reach the right renal artery under fluoroscopy. Super-selective access to the renal artery, approximately 1 cm distally from the ostium, was performed using a 2.4 French microcatheter. Slow controlled administration of microspheres was performed ensuring no reflux into non-catheterized arteries. End-point was fixed to a required volume of 50 μL rather than angiographic end-point to allow a free and homogenous distribution of microspheres within the vessels. The microsphere type was randomized to reduce bias and the procedure was then repeated for the left kidney. All animals were sacrificed by injection of T61® in an earlobe vein under anesthesia, at least 10 min after the second embolization procedure (to allow for any redistribution effects). The two embolized kidneys were sampled, macroscopically examined, photographed then fixed in 10% neutral buffered formalin for at least 24 h.

Tissue specimens were registered with an identification number in order to blind further analyses to the treatment group. On the formalin fixed kidney, 3 tissue slices of 2 cm in thickness were cut radially from the renal hilum (dotted section lines A, B and C on Fig. 4f). Each slice was processed by means of paraffin embedding. Standard hemateine-eosin-saffron (HES) staining was performed and histopathological assessment performed by the same pathologist, recording all of the parameters described in Table 2. These parameters were assessed on 2 tissue sections per kidney and the number of measurements taken was sufficient to perform reliable statistical analysis.

2.7. In vitro in vivo correlation (IVIVC) of microsphere behaviour

Microscopic sizing of LUMI 40–90 and LUMI 70–150 microspheres was performed when confined *in-vitro* within the plate model and compared to the unconfined optically sized microspheres in the petri dish. These values were also compared to the mean reported microsphere diameter measured by histology within the rabbit renal tissue sections. N = 200 measurements were performed evenly across the microsphere distribution band in the plate model for statistical power, ranging from the most distal identified point, to that of the most proximal. The corresponding microsphere location *in vivo* will not only depend upon the size and the compressive modulus differences of the products, but also how they behave when constrained in circular vascular structures. This *in vitro in vivo* comparative assessment will provide a measure of the accuracy of the 2D plate model method for formative *in-vitro* testing of microsphere penetration.

Table 2
Parameters measured for microspheres in the kidney.

Location of the occluded vessels according to a division of the kidney in 5 zones (Laurent *Invest Radiol* 2006; Fig. 4f):
Zone 1: renal artery and its first branches;
Zone 2: interlobar arteries;
Zone 3: junction area at the border of the cortex and medulla, which comprises arcuate arteries, distal part of interlobar arteries and initial interlobular arteries;
Zone 4: deep cortex with proximal interlobular arteries;
Zone 5: superficial cortex with distal interlobular arteries.
Diameter of occluded vessels in histology, measured as the internal lumen diameter of the smallest axis of the vessels occluded by microspheres
Number of microspheres occluding the vessel in the smallest axis of the vessel occluded by beads
Total number of microspheres present in each occluded vessel section in histology
Size (major and minor axis) of the largest microsphere that blocked the vessel
In vivo deformation of the largest microsphere was calculated as follows:
In vivo deformation (%) = $100 \times D_m - minor\ axis / D_m$
where Dm is the mean diameter of the microsphere calculated as the mean between the major and the minor axis of the microsphere.

2.8. Statistical analysis

For the *in-vitro* penetration efficacy evaluations, a Mann-Whitney *U* test was performed on the two non-parametric datasets (n = 200 measurements *in vitro* vs n = 149 *in vivo)* and a line profile was generated for the distal point of penetration (n = 3). For the *in-vivo* microsphere distribution, non-parametric tests were used (Mann-Whitney, Kruskall Wallis, Chi^2, Spearman correlation) for statistical comparison between products or between sizes of each product (Statview 5.0, SAS Institute Inc, Cary, CA USA). Graphs are prepared using GraphPad Prism (Graphpad Software Inc., USA). The level of statistical significance was defined as $p < 0.05$.

3. Results

3.1. Microsphere size, distribution and appearance

Fig. 2 shows optical micrographs for the various embolic microspheres under × 10 magnification. All microspheres appear smooth and spherical in appearance, with EZ 40 tinted black (a), EZ 100 tinted orange (b), LUMI 40–90 (c) and 70–150 (d) a golden color and LC 70–150 tinted blue (e). Fig. 2(f) shows the frequency histograms of each of the produced superimposed on one another. It can be seen that comparing LC 70–150 with LUMI 70–150, the size distribution of the latter is in the same range but skewed to a slightly smaller average diameter (124 μm (range 90–160 μm) *versus* 109.8 μm (range 80–140 μm) respectively). This also compared closely to the EZ 100 product (99.2 μm (range 75.8–121.8 μm)). The LUMI 40–90 has a relatively uniform size, as clearly seen from the optical micrographs in Fig. 2(b) and Table 3. The average size of LUMI 40–90 (63.0 μm (range 41.2–85.8 μm)) is slightly larger than the EZ 40 product (37.9 μm (range = 23.7–53.5 μm)) and both have narrower size distributions

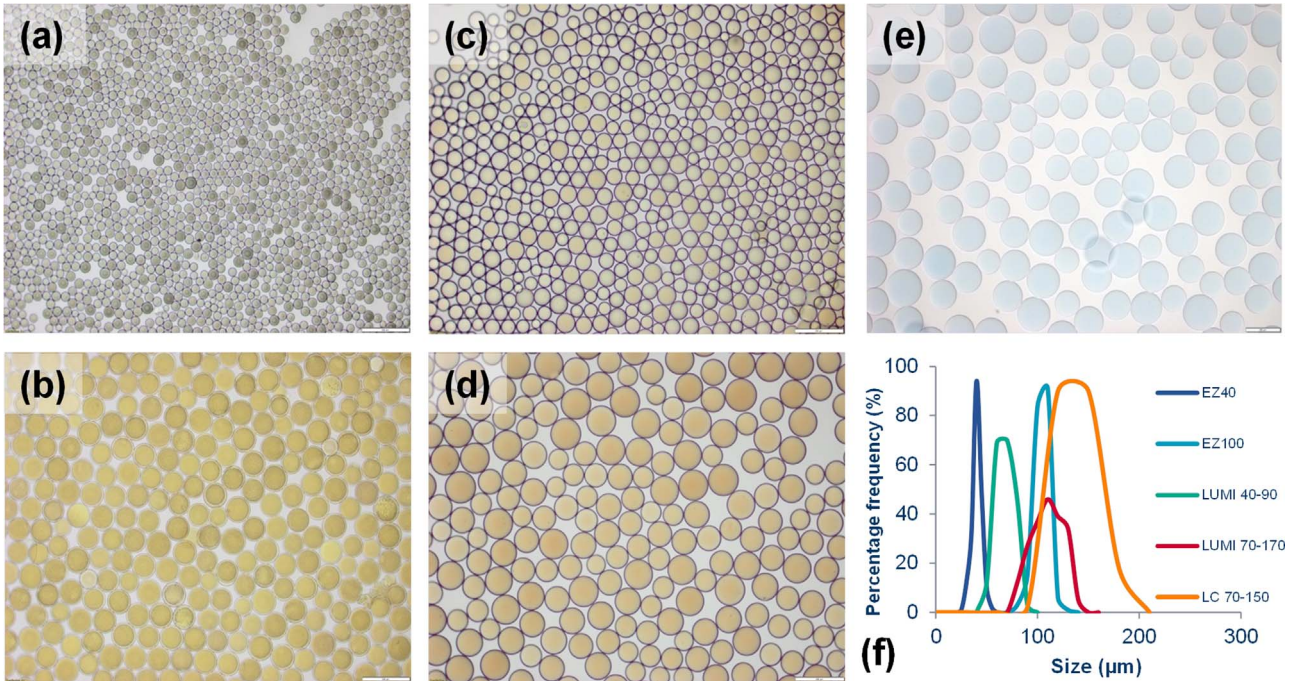

Fig. 2. Optical micrographs (× 10 magnification) of (a) EZ 40, (b) EZ 100, (c) LUMI 40–90, (d) LUMI 70–150, (e) LC 70–150 and (f) the corresponding frequency histogram of the microsphere size distributions.

Table 3
Reported specification, measured size range of microspheres, with the percentage deviation observed during optical microscopy assessment.

Product identifier	Reported size specification (μm)	Measured size range optically (μm)	Deviation outside spec (%)
EZ 40	30–50	24–54	+20 − 8%
LUMI 40–90	40–100	41–86	0%
EZ 100	75–125	76–122	0%
LUMI 70–150	70–170	80–140	0%
LC 70–150	70–170	90–160	0%

than their larger counterparts.

3.2. Evaluation of microsphere physicomechanical properties

Single-bead compression tests were performed on 90–130 μm diameter microspheres within the LC Bead LUMI™ and Embozene™ size ranges under investigation. Typical load-displacement curves for LUMI 70–150 and EZ 100 are shown in Fig. 3. The data are from individual beads and represent typical responses. LUMI 70–150 displays a linear increase in force with displacement. Hysteresis was observed on unloading with a residual displacement at zero force (Fig. 3(a)). The calculated elastic modulus decays with increasing bead compression (Fig. 3(b)). The load-displacement curve is noisier for EZ 100 than LUMI 70–150 due to the 30× lower force (0.5mN *vs* 15mN) required to achieve a similar bead compression (Fig. 3(c)). The unloading curve shows a noticeable residual displacement at zero load but less clearly pronounced than for LUMI 70–150 (Fig. 3(d)).

The average modulus value between 20–30% compression was reported in Table 4 to compare the compressive moduli of the 2 types of microsphere with those reported in previous studies. The compressive modulus of LC Bead LUMI™ was 2 orders of magnitude times greater than that of LC Bead (25,900 kPa *vs* 110 kPa). This single microsphere compression method generates modulus values for LC Bead LUMI™ similar to that reported by Duran et al. (2016) (27,200 kPa *vs* 25,900 kPa who also used a single microsphere method). EZ 100 indicated 10 times stiffer modulus in this side-by-side compression compared to previous reports (Hidaka et al., 2011) (580 kPa *vs* 13.6 kPa). However, this was performed with smaller microspheres (100 μm *vs.* 900 μm) and with single microsphere *vs*. monolayer methods. Clearly LC Bead LUMI™ has a much greater resistance to compression than any of the other microspheres evaluated, regardless of the differences in the methods used.

3.3. 2D plate model distal penetration potential

Fig. 4(a) shows the various embolic microsphere sizes (average diameter, minimum and maximum values) as measured under the optical microscope (unconfined) compared to calculated diameter and range for the same microspheres when delivered into the 2D plate model (Confined). All of the products appear to travel to a slightly more distal position on the plate than anticipated by the minimum size determined optically. Increased penetration or lack of control at the distal end of this size distribution could increase risk of microsphere permeation of the vascular bed or off target embolization (Maluccio et al., 2008). Therefore tight manufacturing control of the lower end of the proposed LUMI 40–90 microspheres is maintained. It is also worth noting that the absolute range of microsphere sizes presented is larger for LC and LUMI 70–150 (100 μm) when compared to LUMI 40–90 (60 μm) and the reported EZ 40 (20 μm), EZ 100 (50 μm) (Table 2), this could be reflected in the increased variation when comparing optical and plate sizes during sampling. If one considers how far the sizes determined from the two methods deviate from the ideal situation (Fig. 4(b) and Table 5) it can be seen there is good overall agreement. The lack of deviation from the ideal line means that there is no appreciable microsphere deformation under the hydrostatic pressure generated in the model. Microsphere penetration potential therefore is dependent mostly upon physical size in this case.

3.4. Microsphere in vivo distribution in the kidney embolization model

Microsphere distribution is shown graphically in Fig. 5 and statistical comparisons of the LUMI microspheres *versus* control products shown in Table 6. The graphs depict the percentage of microspheres measured histologically across the five zones of the kidney, ranging

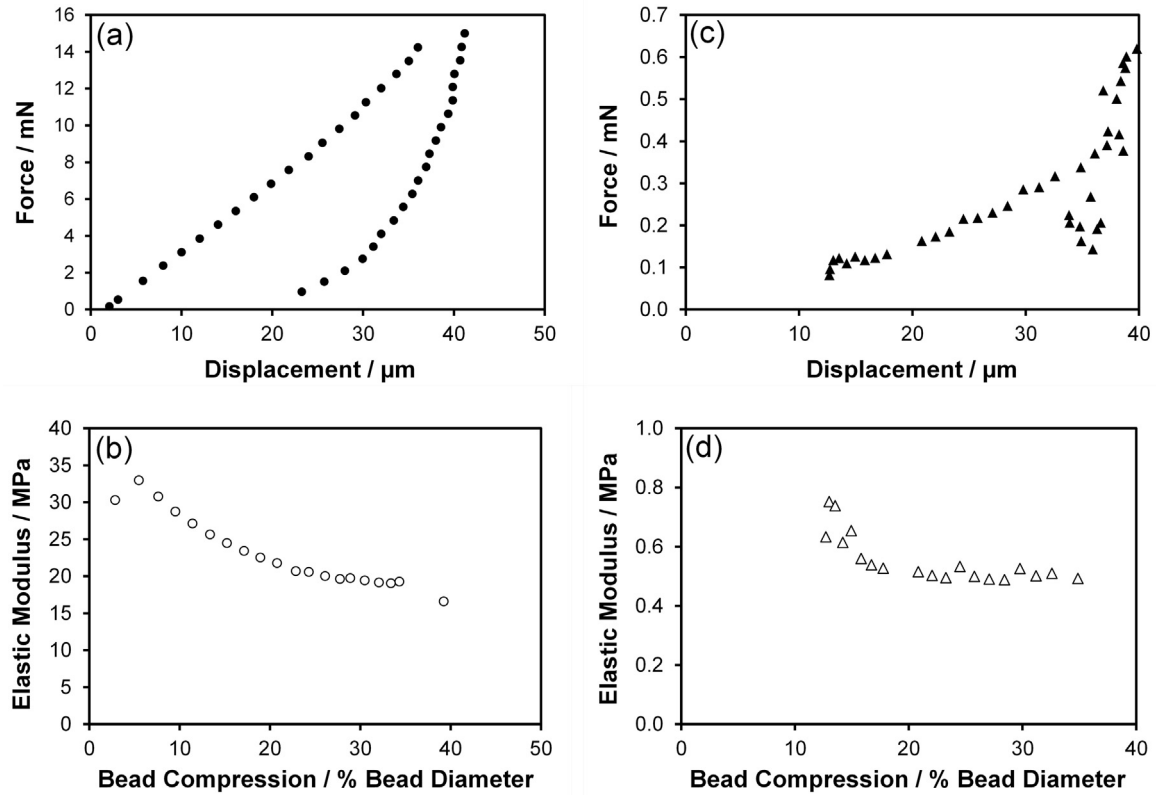

Fig. 3. (a) Load-displacement curve for a typical LUMI 70–150 bead; (b) change in measured Elastic Modulus with extent of bead compression; (c) Load-displacement curve for a typical EZ 100 microsphere; (d) change in measured Elastic Modulus with extent of microsphere compression.

from proximal (renal artery, 3–4 mm) to distal (the superficial cortex with distal interlobular arteries in the range 21–860 µm, see Fig. 5(f)).

When comparing EZ 40–EZ 100 (Fig. 5(a) and (c)) there were more microspheres found in zone 5 for EZ 40 (7% *vs* 17%, the smaller size penetrating more distally) as on average EZ 40 occluded smaller vessels than EZ 100 (66 µm *vs* 85 µm, $p \leq 0.001$). There were also more vessels occluded by multiple microspheres for EZ 40 compared to EZ 100 (37% *vs* 2%) as expected due to the small average size of the product (Fig. 6(a)). The majority of both products was found in similar amounts in zone 4 (74% *vs* 77%) with slightly more microspheres in the proximal zones 1–3 for the larger EZ 100 (9% *vs* 20%).

Similar behaviour was seen when comparing LUMI 40–90 with LUMI 70–150 (Fig. 5(b) and (d), with more LUMI 40–90 in distal zone 5 (27% *vs* 3%), the majority of both products in zone 4 (59% *vs* 77%) and more LUMI 70–150 in the proximal zones 1–3 (15% *vs* 21%). From histopathological assessment it was seen that LUMI 40–90 had a smaller *in vivo* diameter than LUMI 70–150 as anticipated from the size distributions in Fig. 2(f) (median 62 µm *vs* 95 µm respectively). They occluded vessels of smaller diameter (median 77 µm *vs* 110 µm respectively). *In vivo* deformation was very low for both LUMI 40–90 and LUMI 70–150 with no difference between the products (median 2.3% *vs* 2.1% respectively, $p = 0.135$ MW), as can be clearly seen in the

Table 4
Previously reported data for compressive modulus for a range of embolic microspheres.

Product	MS Size (µm)	Test Method	Modulus (kPa)	Reference
LC Bead LUMI™	70–150	Single Bead	25,900 ± 6600	This Study
Embozene™	100	Single Bead	580 ± 190	This Study
LC Bead™	100–300	Single Bead	110 ± 20	Duran, 2016
LC Bead LUMI™	100–300	Single Bead	27,200 ± 5460	Duran, 2016
EmboSphere™	900–1200	Monolayer	39.6 ± 5.05	Hidaka, 2011
Bead Block™	900–1200	Monolayer	18.8 ± 4.00	Hidaka, 2011
Embozene™	900	Monolayer	13.6 ± 1.98	Hidaka, 2011
EmboSphere™	700–900	Single Bead	19.33 ± 4.97	Hidaka, 2010
HepaSphere™	300–350 (dry)	Single Bead	9.64 ± 2.46	Hidaka, 2010
EmboSphere™	900–1200	Monolayer	14.8 ± 0.8	Forster, 2010
Bead Block™	900–1200	Monolayer	11.1 ± 0.8	Forster, 2010
DC Bead™	900–1200	Monolayer	17.1 ± 1.2	Forster, 2010
Contour SE™	900–1200	Monolayer	3.5 ± 1.4	Forster, 2010
DC Bead™	500–700	Monolayer	5.5 ± 0.02	Jordan, 2010
HepaSphere™	100–150 (dry)	Monolayer	1.6 ± 0.3	Jordan, 2010
DC Bead™	700–900	Monolayer	33.0 ± 2.9	Lewis, 2007
EmboSphere™	700–900	Monolayer	27.6 ± 3.8	Lewis, 2006
Bead Block™	700–900	Monolayer	24.1 ± 1.62	Lewis, 2006
Contour SE™	700–900	Monolayer	4.48 ± 1.88	Lewis, 2006
EmboGold™	700–900	Monolayer	21.0 ± 2.48	Lewis, 2006

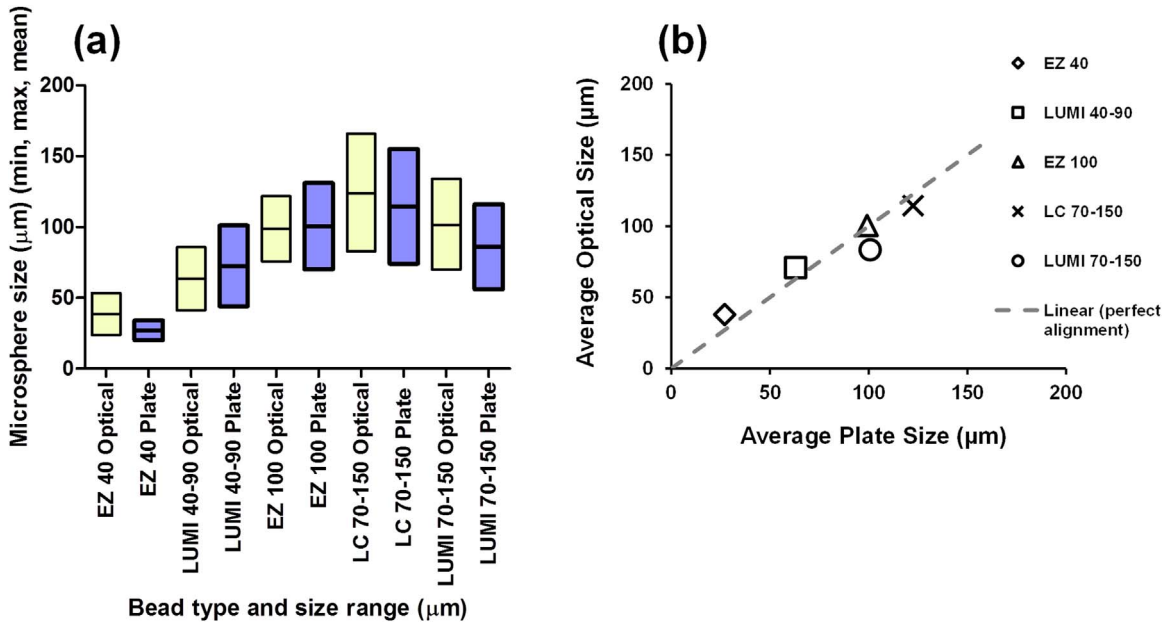

Fig. 4. (a) Microsphere minimum, maximum and mean size measured optically compared to the sizes calculated from the average, distal and proximal positions of the microsphere bands on the 2D plate model n = 3 replicates; (b) comparison of the reported optical "unconfined" average microsphere size and those of the plate "confined". Linear hashed line indicates method alignment; deviation below the line indicates higher reported size in plate model with deviation above indicating larger reported size in optical measurements.

Table 5
Average, maximum and minimum size (μm) reported from optical sizing and plate model experiments. N = 3 replicates for each experiment and product type.

	Product identifier				
Optical Size	EZ 40	LUMI 40–90	EZ 100	LUMI 70–150	LC 70–150
Average (μm)	37.9	63	99.2	109.8	125
Max (μm)	53.5	85.8	121.8	140	160
Min (μm)	23.7	41.2	75.8	80	90
Plate size					
Average (μm)	27	72.5	100.5	83.5	114.5
Max (μm)	34	101	131	120	155
Min (μm)	20	44	70	47	74

histological sections in Fig. 6(c) and (d)).

When comparing EZ 40 and LUMI 40–90 (Fig. 5(a) and (b)), distribution patterns were similar, although slightly more product resided in the more distal zone 5 for LUMI 40–90 compared to EZ 40 making this difference significant ($p = 0.008$). Minimum diameter of occluded vessels was statistically different between LUMI 40–90 and EZ 40 (77 μm *vs* 66 μm, $p \leq 0.001$), as was *in vivo* microsphere minimum diameter (37 μm *vs* 17 μm, $p \leq 0.001$) which may be due to the overall smaller diameter and fraction of very small microspheres detected within the EZ 40 product.

Comparing EZ 100, LUMI 70–150 and LC 70–150 (Fig. 5(c), (d) and (e)), the microsphere distributions were almost identical for all products (no statistical differences), suggesting that although the average size and distribution for these products are slightly different (Fig. 2(f)), their penetration potential and *in vivo* distribution profiles are very similar (as vessel sizes *in vivo* are also a distribution of sizes). The diameter of occluded vessels was however significantly larger for LUMI 70–150 compared to LC 70–150 and EZ 100 (median 110 μm *vs* 92 μm and 85 μm respectively), possibly due to the lower *in vivo* deformation of the LUMI product (median 2.1% *vs* 6.4% and 6.2% respectively, $p \leq 0.001$ MW) or the higher percentage of vessels occluded by multiple microspheres for LUMI 70–150 (18% *vs* 2% and 2% respectively). The average *in vivo* microsphere diameter was statistically smaller for EZ 100 compared to LC 70–150 and LUMI 70–150 (56 μm vs 89 μm and 95 μm) as can be clearly seen on the histology sections (Fig. 7(b) vs (d) and (e)). The reason for this is unclear, given the size distributions are similar between the three products (Fig. 2(f)).

3.5. In vitro- in vivo correlation

Comparison was made between the microsphere penetration potential *in vitro* (average size of the embolized section with sizes at the proximal and distal locations) from the 2D plate model *versus* the average microsphere diameter measured *in vivo*, together with minimum and maximum microsphere sizes measured (Fig. 7). The *in vitro* model provides a good predictor of the microsphere size and distribution expected *in vivo*. For both LC 70–150 and EZ 100, smaller microsphere sizes were observed *in-vivo* than predicted by the distribution on the plate model; this may be due to the increased deformation observed *in-vivo* for these products which have an inherently lower compressive modulus compared to the LUMI microspheres (Table 4). Notwithstanding, there is good agreement between the 2D plate model and *in vivo* results with at most 29 μm variation from plate model to scaled renal vasculature and moreover, the model is consistent as successive experimental replicates using the same batch of microspheres yield no statistical difference (Fig. 6(b)).

4. Discussion

When embolizing a vessel, embolic agents are selected on the basis of their size. Most products are provided as a distribution of sizes over a particular range, where the minimum, maximum and breadth of that range varied from one product to the next. In addition to size and distribution range, the mechanical properties of the microspheres are also important parameters in how they will behave during use. Ideally, larger size microspheres need to be compressible enough to deform and allow delivery through narrow lumen microcatheters. This is not so important for smaller diameter microspheres, although specific guidance in terms of dilution, suspension and delivery should be followed for products with high density to prevent microspheres occluding the catheter lumen.

In order to gain an appreciation of the mechanical properties of the microspheres, many different techniques have been employed in order to compress either a monolayer of microspheres, or in some cases, individual microspheres themselves. Table 4 lists the mechanical

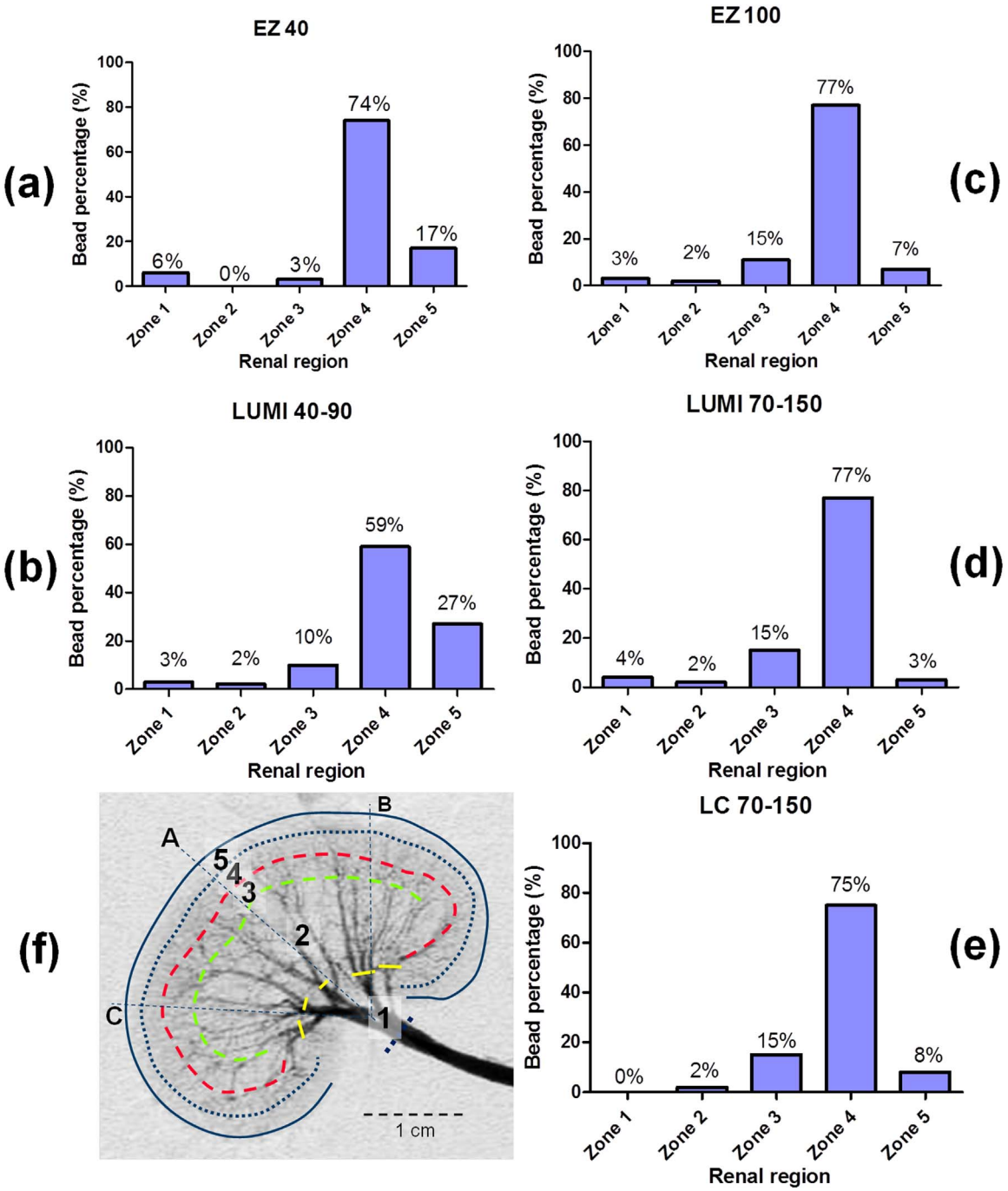

Fig. 5. Microsphere distribution patterns across the zones of the kidney for EZ 40 (a), LUMI 40–90 (b), EZ 100 (c), LUMI 70–150 (d), LC 70–150 (e). Arteriogram of a kidney demonstrating the different arterial zones (f). Smaller microspheres have a higher penetration into the more distal zone 5 than larger microspheres.

Table 6
Statistical *p* values (Chi^2 and Mann-Whitney U, n = 149) between selected *in vivo* attributes assessment of test articles.

	LUMI 40–90 vs EZ 40	LUMI 40–90 vs EZ 100	LUMI 40–90 vs LC 70–150	LUMI 70–150 vs EZ40	LUMI 70–150 vs EZ100	LUMI 70–150 vs LC 70–150
Location	0.008	0.001	0.018	< 0.001	0.614	0.318
Vessel diameter	< 0.001	0.103	0.012	< 0.001	< 0.001	< 0.001
Microsphere diameter	< 0.001	0.018	< 0.001	< 0.001	< 0.001	0.195
Microsphere deformation	0.902	< 0.001	< 0.001	0.220	< 0.001	< 0.001
Nb microspheres in vessel	0.050	< 0.001	< 0.001	0.056	< 0.001	< 0.001
Nb microspheres occluding vessel	0.030	0.050	0.078	0.046	0.047	0.073

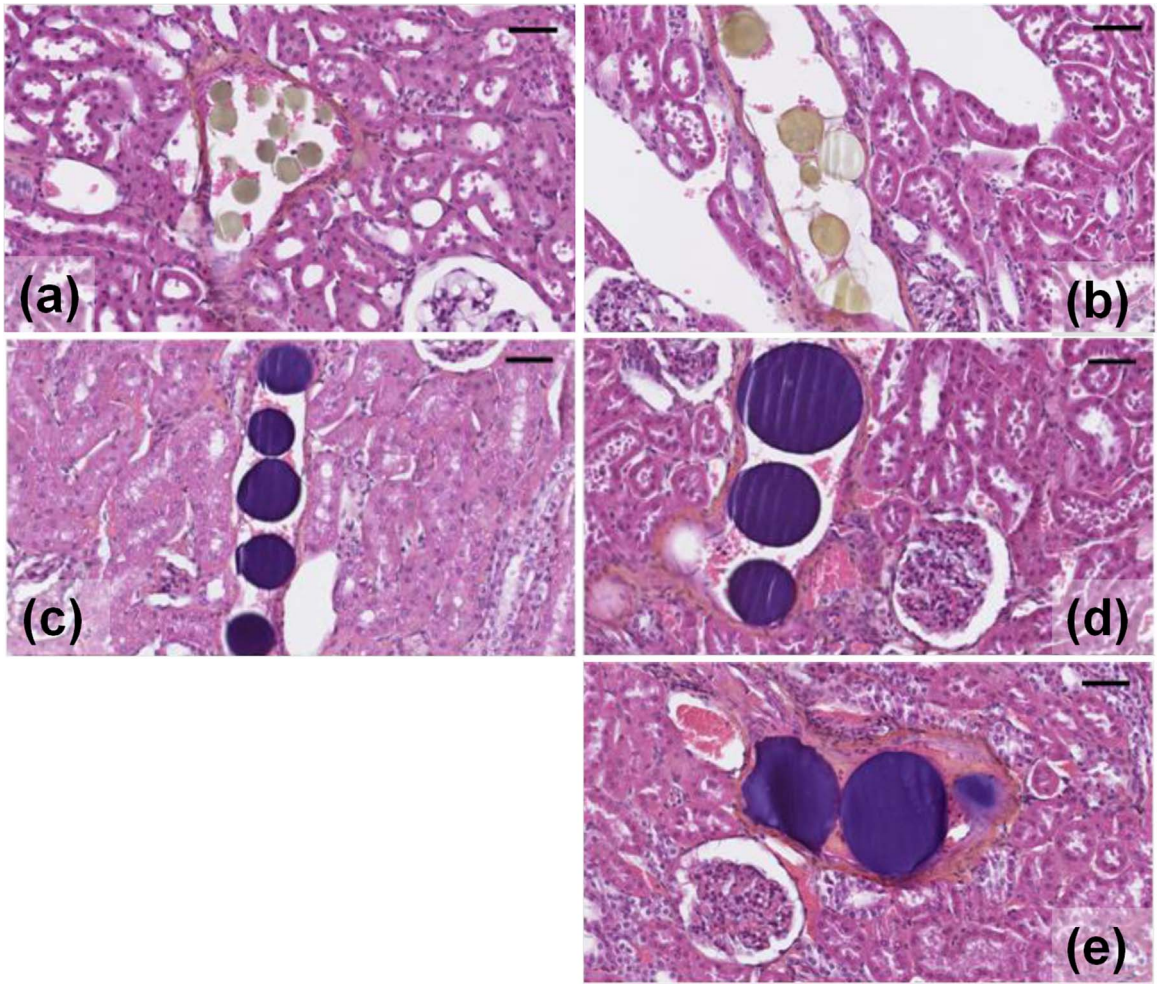

Fig. 6. Representative histological sections (H&E staining) showing the various microspheres within the vessels of the kidney: (a) EZ 40; (b) EZ 100; (c) LUMI 40–90; (d) LUMI 70–150; (LC 70–150). Scale bar = 50 μm.

properties of some of the common commercially-available embolic microspheres that have been reported in the literature, expressed as the compressive modulus (measured in kPa). A number of features are apparent from this list: (i) Tests performed on the same product but by different investigators yield data of a similar order of magnitude but the absolute value recorded for a specific microsphere is different between studies. (ii) Even when tests are performed by the same investigators, when comparing methods that compress single microspheres *versus* those that compress a monolayer, the absolute value for the modulus of a particular microsphere is different. (iii) Bead size may be an influencing factor. Larger beads are more easily measured, whereas ~ 150 μm microspheres are the smallest that have been accurately measured, but even then with some difficulty.

The time-dependent nature of the mechanical response of polymeric materials, such as these hydrogel microspheres, means that they do not have a unique value for their elastic modulus. The value obtained also depends on the test conditions such as load rate and deformation rate. The time-dependent materials response may arise from three different phenomena such as, visco-elastic (time-dependent, reversible deformation), visco-plastic (time-dependent viscous flow), and poroelastic (time-dependent flow of liquid in a porous elastic medium). The LUMI load-displacement curve showed a linear increase in force with displacement, which is not expected from Hertzian elastic contact mechanics where force is proportional to displacement to power 1.5. This indicates that the material response is not linear-elastic but relaxes during compression. The bead displays viscoelastic recovery, as indicated by the hysteresis on unloading, and possibly a small time-dependent permanent deformation over the time scale of the measurement (~ 20 s). The time-dependent response will also affect the loading curve, so that the calculated elastic modulus appears to reduce with deformation of the bead as it relaxes over time (Fig. 3(b)). For EZ 100, the minimum force required to reliably detect the surface of the bead resulted in a displacement of 10 μm before force-displacement data could be collected. Compressions of greater than 30% of the diameter were achieved with 0.5mN forces. The force-displacement data shows a more Hertzian elastic response, curving upwards during loading. However, the unloading response does not show elastic recovery, possibly indicating adhesion between the bead and the flat punch. The EZ 100 beads display an approximately 30% higher elastic modulus at bead compressions less than 15% of the diameter. At compressions higher than 15%, the elastic modulus appears to be constant. This is different to the response of the LUMI 70–150, where the elastic modulus continues to decay with increasing compression. For the EZ 100 this could indicate a core-shell behaviour (see Fig. 2b), where the surface is stiffer than the bulk. The EZ 100 compressive modulus was much lower than for LUMI 70–150 (0.58 ± 0.19 MPa *vs* 25.9 ± 6.0 MPa) but is far higher than previously reported by others (Table 4). This clearly demonstrates that the measured mechanical properties are highly dependent upon the applied technique, including factors such as the rate and extent of compression and the method employed to extract the elastic modulus from the data. Ideally, elastic modulus values should be compared from similar methodologies. Bearing in mind this variation, comparing the compressive modulus values can be insightful for bench-marking different embolic products.

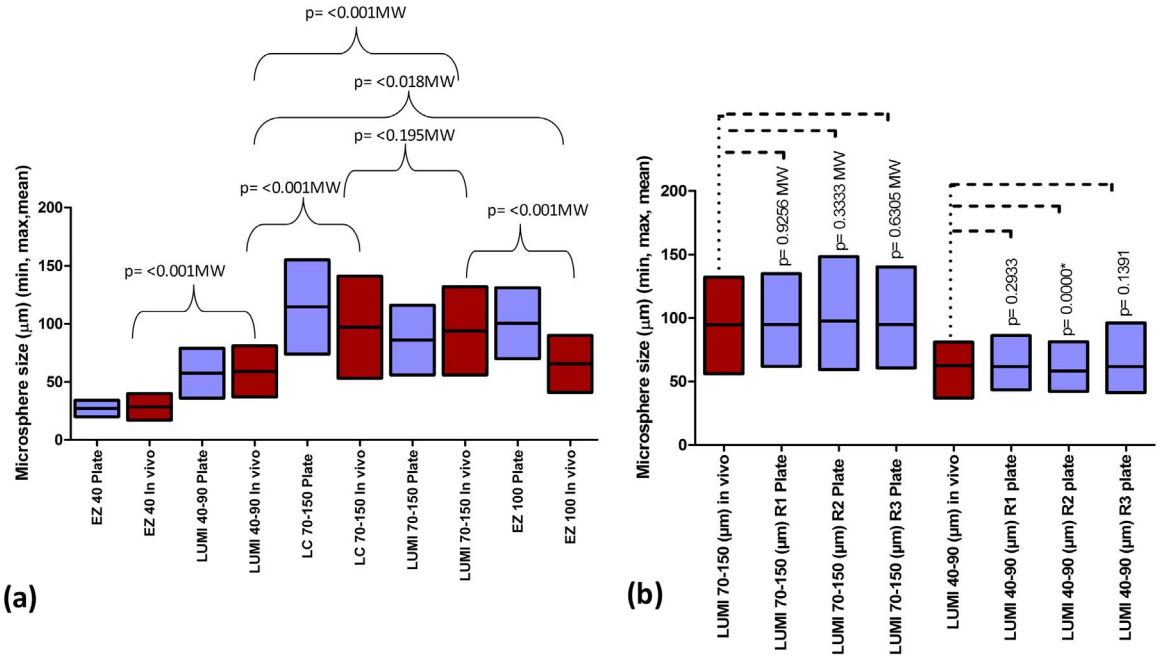

Fig. 7. (a) Comparison of the microsphere location on the 2D plate model *versus* the corresponding average, minimum and maximum microsphere size measured in histopathology in the kidney and statistical comparisons between microsphere *in vivo* distributions; (b) *in vivo* microsphere min, max and mean for LUMI 70–150 (n = 149) and LUMI 40–90 (n = 125) (red boxes) *versus* 2D model plate model predicted min, max and mean sizes (blue boxes) (n = 200, n = 3 replicates for each size range) demonstrating consistency of the model and showing general profile for no statistical difference between the *in-vivo* and *in vitro* results (MW p = > 0.05), exception is replicate 2 of LUMI 40–90 with p = 0.001, however, the average profile supports equivalence within the size range. (For interpretation of the references to color in this figure legend, the reader is referred to the web version of this article.).

For instance, in Table 4 it is clear from the comparison of the products tested by both Lewis 2006 and Forster 2010 that the modulus of Contour SE seems significantly lower than the other embolic microspheres tested, which may raise questions about this products behaviour *in vivo*. Indeed, the clinical literature reported of the difficulties experienced with the use of this product with inadequate devascularisation as a result of its softness, lack of shape recovery and more distal migration (Spies et al., 2005; Siskin et al., 2008).

For LC Bead LUMI™, the increase in density of the product due to the attachment of the iodine to the structure means that the mechanical properties are increased and the compressive modulus is significantly higher than any of the currently-available embolic microspheres (Table 3). Taken in isolation, this might lead to concerns about the increase in stiffness affecting the ability to deliver the product through a microcatheter and preventing deeper penetration into the vasculature as the product will deform less than conventional microspheres. We have recently reported on a new method that was developed to better assess the penetration potential for embolic microspheres by monitoring the flow of the product through a device with a wedge-shaped gap geometry, whereby the microspheres become trapped under a glass window according to their size and ability to deform under physiologically-relevant flow pressures. When LC Bead LUMI™ (70–150 µm) is evaluated in this model, it forms a band between 56 µm and 116 µm, similar to EZ 100 µm and LC 70–150 µm albeit with slightly more distal penetration. Therefore, in this model, the significant increase in the compressive modulus of LC Bead LUMI™ is not affecting its ability to travel more distally under fluid pressure representative of that experienced in the arteries. LC Bead LUMI™ (40–90 µm) penetrates more distally than LUMI 70–150 and forms a narrower band between 36 µm and 79 µm. EZ 40 µm penetrates the most distally, with a narrow band from 20 to 34 µm, somewhat more distal than predicted from the labelled size. Additionally, a small band of product around 15–20 µm could be seen accumulating on the plate model and corresponds to the small microsphere population measured using optical microscopy that has been observed in some batches of this product. Others have also previously reported on the Embozene™ product size distribution not being as narrowly calibrated as claimed on the product label (Verret et al., 2011).

The data from this investigation confirmed that the rabbit renal artery embolization model was sufficiently sensitive to distinguish between the distribution patterns and depth of penetration for the smaller *versus* larger microsphere types (40–90 µm *vs* 70–150 µm), through the determination of location of occluded vessels, diameter of occluded vessels, number of microspheres occluding vessels, size and *in vivo* microsphere deformation. The *in vivo* data showed that despite the more rigid modulus for the LC Bead LUMI™ microspheres, their distribution patterns across the different vascular zones in the kidney were comparable to similarly-sized commercially available control microsphere (LUMI 40–90 comparable to EZ 40 and LUMI 70–150 comparable to both EZ 100 and LC 70–150).

IVIVC performed by analysis of the location of different microspheres in the plate model with that of the microspheres within the kidney shows on average, no gross statistical difference (Mann-Whitney U, n = 3 replicates: p = > 0.05 n = 149 (70–150 µm) and n = 125 (40–90 µm) data *vs* n = 200 plate model) Fig. 7b. This indicates that the final distal position and size of the microspheres studied could be predicted through the use of this applied *in vitro* model. The model offers a method for evaluation of smaller size fractions that removes the limitations experienced in traditional bi-axial compression methods. Moreover, the model predicts that once a threshold compressive modulus has been reached, the microspheres resistance to compression is no longer as important an influencer of occlusion location as the size of the microsphere. That is because the pressures the microspheres experience within the blood vessels during and post-embolization are insufficient to deform the microspheres enough to induce further migration or redistribution; unlike much softer microspheres which can demonstrate such phenomena due to changes in dimension during delivery and under pressure in the vessels.

5. Limitations

Although the various microspheres used had similar size

distributions, the use of the kidney embolization model is associated with several limitations. For this study it was decided to deliver a set volume of microspheres into the kidney rather than deliver to an angiographic endpoint such as stasis, which is more representative of clinical practice and could potentially influence the depth of penetration of the products into the vascular tree. The microsphere diameter measured *in vivo* is always under-reported when determined by histological sectioning as there is limited chance a section will fall through the exact centre of the microsphere. There is obviously potential bias in obtaining a representative distribution of the microspheres across the entire kidney based on a limited number of histological sections but this model has been reported on several occasions and appears to allow statistically meaningful comparisons to be made (Laurent et al., 2006; Weng et al., 2013; Maeda et al., 2013b). Compression testing limitations are highlighted through analysis of previous study variation as described in Table 4. The 2D plate model also presents several limitations, the geometry of which is rectangular rather than circular and not composed of/ or containing organic tissue/fluids. The influence on adhesion properties could influence overall penetration prediction. No element of vascular inflammation is assessed *in vitro*. The flow properties of the microspheres in terms of compatibility with microcatheters and embolic flow restriction were also evaluated *in vitro,* however this investigation focused on final embolic location rather than transient flow properties therefore data is not presented herein.

6. Conclusions

Mechanical testing of embolization microspheres, whilst valuable when used in comparative testing of products, cannot in isolation provide sufficient predictive information on how the product will penetrate the vasculature. The 2D plate model provides an additional level of information that takes into account the size and size distribution of the microspheres, as well as their tendency to compress in two dimensions under pressures normally experienced within the blood vessels. The penetration potential of the microspheres observed using this method correlate very well with microsphere distribution data generated in the kidney embolization model, which makes the model a valuable addition to the preclinical formative testing package used in the development of novel embolization microsphere products.

Two sizes of LC Bead LUMI™ (40–90 μm and 70–150 μm) and three other commercially-available microspheres (Embozene™ 40 μm, 100 μm and LC Bead*M1*® (70–150 μm)) were optically sized, their compressive modulus measured and penetration potential evaluated in the 2D plate model. Despite much higher compressive moduli recorded for the LC Bead LUMI™ products, their behaviour in the plate model was similar to their analogous sized more compressible counterparts. This finding was corroborated *in vivo* in the kidney embolization model where microsphere distribution patterns were essentially the same for the similar sized products.

Acknowledgements

The authors would like to acknowledge Archimmed SARL and specifically Prof. Alexandre Laurent and Dr. Julien Namur for conducting the rabbit kidney embolization study and pathological analyses.

References

Caine, M., Garcia, P., Tang, Y., Willis, S.L., Dreher, M.R., Lewis, A.L., editor. *In vitro* methods for evaluation of novel Radiopaque Bead flow properties. In: Biomaterials conference 2016. OMICS, London, 2016.

Duran, R., Sharma, K., Dreher, M.R., Ashrafi, K., Mirpour, S., Lin, M., et al., 2016. A novel inherently radiopaque bead for transarterial embolization to treat liver cancer - a preclinical study. Theranostics 6 (1), 28–39 (Epub 2016/01/02).

Forster, R.E., Thurmer, F., Wallrapp, C., Lloyd, A.W., Macfarlane, W., Phillips, G.J., et al., 2010. Characterisation of physico-mechanical properties and degradation potential of calcium alginate beads for use in embolisation. J. Mater. Sci. Mater. Med. 21 (7), 2243–2251 (Epub 2010/04/23).

Hidaka, K., Nakamura, M., Osuga, K., Miyazaki, H., Wada, S., 2010. Elastic characteristics of microspherical embolic agents used for vascular interventional radiology. J. Mech. Behav. Biomed. Mater. 3 (7), 497–503 (Epub 2010/08/11).

Hidaka, K., Moine, L., Collin, G., Labarre, D., Grossiord, J.L., Huang, N., et al., 2011. Elasticity and viscoelasticity of embolization microspheres. J. Mech. Behav. Biomed. Mater. 4 (8), 2161–2167 (Epub 2011/11/22).

Jordan, O., Denys, A., De Baere, T., Boulens, N., Doelker, E., 2010. Comparative study of chemoembolization loadable beads: in vitro drug release and physical properties of DC bead and hepasphere loaded with doxorubicin and irinotecan. J. Vasc. Interv. Radiol. 21 (7), 1084–1090 (Epub 2010/07/09).

Khurana, I., 2006. In: Circulation, R. (Ed.), Textbook of Medical Physiology. Elsevier, Dehli, India, pp. 383.

Laurent, A., Wassef, M., Saint Maurice, J.P., Namur, J., Pelage, J.P., Seron, A., et al., 2006. Arterial distribution of calibrated tris-acryl gelatin and polyvinyl alcohol microspheres in a sheep kidney model. Investig. Radiol. 41 (1), 8–14 (Epub 2005/12/16).

Levy, E.B., Krishnasamy, V.P., Lewis, A.L., Willis, S., Macfarlane, C., Anderson, V., et al., 2016. First human experience with directly image-able iodinated embolization microbeads. Cardiovasc. Interv. Radiol. 39 (8), 1177–1186 (Epub 2016/05/22).

Lewis, A.L., Adams, C., Busby, W., Jones, S.A., Wolfenden, L.C., Leppard, S.W., et al., 2006. Comparative in vitro evaluation of microspherical embolisation agents. J. Mater. Sci. Mater. Med. 17 (12), 1193–1204 (Epub 2006/12/05).

Lewis, A.L., Gonzalez, M.V., Leppard, S.W., Brown, J.E., Stratford, P.W., Phillips, G.J., et al., 2007. Doxorubicin eluting beads – 1: effects of drug loading on bead characteristics and drug distribution. J. Mater. Sci. Mater. Med. 18 (9), 1691–1699 (Epub 2007/05/08).

Lewis, A.L., Dreher, M.R., O'Byrne, V., Grey, D., Caine, M., Dunn, A., et al., 2016. DC BeadM1™: towards an optimal transcatheter hepatic tumour therapy. J. Mater. Sci.: Mater. Med. 27 (1), 1–12.

Maeda, N., Verret, V., Moine, L., Bédouet, L., Louguet, S., Servais, E., et al., 2013a. Targeting and recanalization after embolization with calibrated resorbable microspheres versus hand-cut gelatin sponge particles in a porcine kidney model. J. Vasc. Interv. Radiol. 24 (9), 1391–1398.

Maeda, N., Verret, V., Moine, L., Bedouet, L., Louguet, S., Servais, E., et al., 2013b. Targeting and recanalization after embolization with calibrated resorbable microspheres versus hand-cut gelatin sponge particles in a porcine kidney model. J. Vasc. Interv. Radiol. 24 (9), 1391–1398 (Epub 2013/07/31).

Maluccio, M.A., Covey, A.M., Porat, L.B., Schubert, J., Brody, L.A., Sofocleous, C.T., et al., 2008. Transcatheter arterial embolization with only particles for the treatment of unresectable hepatocellular carcinoma. J. Vasc. Interv. Radiol. 19 (6), 862–869.

Sharma, K.V., Bascal, Z., Kilpatrick, H., Ashrafi, K., Willis, S.L., Dreher, M.R., et al., 2016. Long-term biocompatibility, imaging appearance and tissue effects associated with delivery of a novel radiopaque embolization bead for image-guided therapy. Biomaterials 103, 293–304 (Epub 2016/07/16).

Siskin, G.P., Beck, A., Schuster, M., Mandato, K., Englander, M., Herr, A., 2008. Leiomyoma infarction after uterine artery embolization: a prospective randomized study comparing tris-acryl gelatin microspheres versus polyvinyl alcohol microspheres. J. Vasc. Interv. Radiol. 19 (1), 58–65 (Epub 2008/01/15).

Spies, J.B., Allison, S., Flick, P., Cramp, M., Bruno, J., Jha, R.C., et al., 2005. Spherical polyvinyl alcohol versus tris-acryl gelatin microspheres for uterine artery embolization for leiomyomas: results of a limited randomized comparative study. J. Vasc. Interv. Radiol. 16 (11), 1431–1437 (Epub 2005/12/02).

Stampfl, S., Bellemann, N., Stampfl, U., Sommer, C.M., Thierjung, H., Lopez-Benitez, R., et al., 2009. Arterial distribution characteristics of Embozene particles and comparison with other spherical embolic agents in the porcine acute embolization model. J. Vasc. Interv. Radiol. 20 (12), 1597–1607 (Epub 2009/12/01).

Verret, V., Ghegediban, S.H., Wassef, M., Pelage, J.P., Golzarian, J., Laurent, A., 2011. The arterial distribution of embozene and embosphere microspheres in sheep kidney and uterus embolization models. J. Vasc. Interv. Radiol. 22 (2), 220–228 (Epub 2011/02/01).

Weng, L., Rusten, M., Talaie, R., Hairani, M., Rosener, N.K., Golzarian, J., 2013. Calibrated bioresorbable microspheres: a preliminary study on the level of occlusion and arterial distribution in a rabbit kidney model. J. Vasc. Interv. Radiol. 24 (10), 1567–1575.